Atmos. Chem. Phys., 25, 17125–17138, 2025 https://doi.org/10.5194/acp-25-17125-2025 © Author(s) 2025. This work is distributed under the Creative Commons Attribution 4.0 License.





Atmospheric new particle formation in the eastern region of China: an investigation on mechanism and influencing factors at multiple sites

Jiaqi Jin 1 , Runlong Cai 1,2,3,4 , Yiliang Liu 1,a , Gan Yang 1 , Yueyang Li 1 , Chuang Li 1 , Lei Yao 1,2,3,4 , Jingkun Jiang 5,6 , Xiuhui Zhang 7 , and Lin Wang 1,2,3,4,8

¹Department of Environmental Science and Engineering, Jiangwan Campus, Shanghai Key Laboratory of Atmospheric Particle Pollution and Prevention (LAP³), Fudan University, Shanghai 200438, China
 ²Shanghai Institute of Pollution Control and Ecological Security, Shanghai 200092, China
 ³IRDR International Center of Excellence on Risk Interconnectivity and Governance on Weather/Climate Extremes Impact and Public Health, Fudan University, Shanghai, China

⁴National Observations and Research Station for Wetland Ecosystems of the Yangtze Estuary, Shanghai, China ⁵State Key Joint Laboratory of Environmental Simulation and Pollution Control, School of Environment,

Tsinghua University, Beijing, China

⁶State Environmental Protection Key Laboratory of Sources and Control of Air Pollution Complex, Beijing, China

⁷Key Laboratory of Cluster Science, Ministry of Education of China, School of Chemistry and Chemical Engineering, Beijing Institute of Technology, Beijing, China

⁸Collaborative Innovation Center of Climate Change, Nanjing, 210023, China

^anow at: Chongqing Institute of Green and Intelligent Technology, Chinese Academy of Sciences, Chongqing 400714, China

Correspondence: Lin Wang (lin_wang@fudan.edu.cn)

Received: 12 June 2025 – Discussion started: 4 July 2025 Revised: 4 November 2025 – Accepted: 5 November 2025 – Published: 28 November 2025

Abstract. As a major source of cloud condensation nuclei, atmospheric new particle formation (NPF) events exert significant influences on the global climate. Among nucleation mechanisms identified in diverse environments, sulfuric acid-amine nucleation is unique for its high efficiency in forming stable clusters and driving intense nucleation. Despite the fact that this nucleation mechanism can explain observed NPF events at individual sites, its applicability to a larger regional scale remains unclear. Here, we analyze the mechanism and influencing factors of NPF at several sites in the eastern region of China, using measured and theoretically predicted particle formation rates and cluster concentrations. Results show that sulfuric acid and dimethylamine can explain the observed atmospheric nucleation and atmospheric conditions including precursor concentrations and temperature cause the differences in NPF characteristics among sites. This indicates the significance of the sulfuric acid-amine nucleation over a large spatial scale in polluted and populated regions. We also find that oxygenated organic molecules are likely involved in the formation of 1.7 nm new particles at these sites by contributing the initial growth of stable sulfuric acid clusters.

1 Introduction

New particle formation (NPF), an important atmospheric process involving the conversion of gaseous precursors into stable clusters via nucleation and subsequent growth, occurs frequently in diverse environments (Kerminen et al., 2018). It is a large source of the number concentration of atmospheric particles and significantly influences the budget of global cloud condensation nuclei (Gordon et al., 2017). Among a number of recently proposed nucleation mechanisms (Kirkby et al., 2023), the collision between sulfuric acid (SA) and dimethylamine (DMA) is special for its high efficiency in forming clusters that are stable against evaporation, and has been found to be the governing nucleation mechanism in polluted megacities (Yao et al., 2018; Cai et al., 2021). These findings corroborated prior studies conducted in urban Tecamac (Smith et al., 2010) and Atlanta (Hanson et al., 2011), where aminium salts were identified as a dominant constituent of particles below 10 nm. Despite substantial suppression by background aerosols, strong NPF events were observed globally in polluted environments, though the underlying mechanisms often remain unclear (Nieminen et al., 2018). A recent model study (Zhao et al., 2024) indicated that SA-amine was the main nucleation mechanism in the polluted atmospheric boundary layers across larger regions. However, this regional-scale dominance requires evidence from field measurements.

Atmospheric NPF is often a regional-scale phenomenon spanning hundreds of kilometers (Kerminen et al., 2018). Simultaneous measurements at two or more stations have demonstrated the spatial heterogeneity of regional NPF characteristics such as event frequency, start time, duration, and the formation and growth rates of new particles (Bousiotis et al., 2021; Zhou et al., 2021; Dinoi et al., 2023). This heterogeneity of NPF may be associated with the spatially variable distributions of emission sources, complex morphology and meteorology, and the strong selectivity and sensitivity of NPF to atmospheric conditions. The main causes of variations in the macroscopic characteristics of NPF require further verification, necessitating mechanistic investigations across large regions.

A number of influencing factors need to be accounted for when resolving nucleation mechanisms in the real atmosphere. Besides the concentrations of gaseous precursors and the scavenging loss of clusters and particles characterized by the condensation sink (CS), temperature effects on cluster stability against evaporation (Olenius et al., 2017; Li et al., 2023). A global simulation study suggested that temperature was the second most important factor in nucleation, following the concentration of precursors (Zhao et al., 2024). Laboratory studies provided experimental evidence for the dependence of sulfuric acid-amine nucleation on temperature at atmospheric-relevant amine concentrations (Xiao et al., 2021). Previous 1 year measurements in urban Beijing showed that temperature governed seasonal variations

of NPF frequency and particle formation rate (Deng et al., 2020). This also indicates that the intensity and characteristics of NPF likely vary on a large spatial scale, e.g., the characteristics of NPF in temperate (Cai et al., 2021) and tropics (Sebastian et al., 2021) regions can be different, even though the NPF events were governed by the same nucleation mechanisms

The initial growth of freshly nucleated particles is important for NPF, as these smallest particles are highly susceptible to scavenging losses. Previous studies proposed that SA and its clusters significantly contributed to the initial growth in urban areas, although contributions of other condensable vapors, like oxygenated organic molecules (OOMs), could not be excluded (Yao et al., 2018; Deng et al., 2020). OOMs are identified as highly important precursors for the subsequent growth of particles. Observational evidence from remote forests suggested that the volatility distribution of OOMs reasonably accounted for particle growth from 3 to 50 nm (Mohr et al., 2019). Similarly, in urban environments, a substantial fraction of particle growth above 3 nm was attributed to the condensation of OOMs (Qiao et al., 2021), indicating their key role in both anthropogenically influenced and natural settings. Moreover, insights from chamber studies further supported the potential role of OOMs in growth of newly formed particles. Some extremely low-volatility OOMs can promote directly to the initial growth of particles below 3 nm (Tröstl et al., 2016; Stolzenburg et al., 2018). Laboratory results indicated that OOMs contributions to the initial growth of new particles are likely non-negligible in the real atmosphere, however, ambient evidence for this process remains limited.

To deepen the understanding of NPF in polluted atmospheres, we collected data measured at three suburban sites and two urban sites in the eastern part of China, including SA and DMA concentrations ([SA] and [DMA]), OOMs concentrations ([OOMs]), cluster compositions, and particle size distribution (PSD) down to $\sim 1\,\mathrm{nm}$. The nucleation mechanisms were analyzed after accounting for the effects of temperature and precursor concentrations on cluster concentrations and particle formation rates. Additionally, we investigated the initial growth of new particles and explored the roles of OOMs in the formation of 1.7 nm particles.

2 Methods

2.1 Measurements

We conducted field campaigns at three suburban sites, namely Wangdu (WD), Dianshan Lake (DL) and Taihu Lake (TL). WD is located in Baoding, Hebei, with farmlands, forests and two major roads nearby. DL is located in the southwest of Shanghai, surrounded by residential buildings, vegetation, a highway and a few industrial enterprises. Two campaigns were conducted at DL, one in winter (DLW) and the other in spring (DLS). TL is located in Wuxi, Jiangsu,

surrounded by vegetation and a small number of settlements. The detailed information of these campaigns is given in Table 1. Furthermore, this study also involves ambient data previously reported from urban sites, namely Shanghai (SH, Yao et al., 2018) and Beijing (BJ, Cai et al., 2021; Qiao et al., 2021). The location of these five sites is shown in Fig. S1 in the Supplement.

A chemical ionization long time-of-flight mass spectrometer (CI-LToF-MS, Aerodyne Research, Inc.) was deployed to measure gaseous SA, OOMs, and molecular clusters at three suburban sites (Lu et al., 2020), using nitrate and its clusters to ionize neutral molecules and clusters. A calibration coefficient derived from SA and a mass-to-charge-dependent transmission efficiency of the instrument were used to obtain [OOMs], assuming that they share the same kinetically controlled collision rate with reagent ions as that of SA. The transmission efficiency was calibrated using a system coupling a high-resolution differential mobility analyzer (HR-DMA) with the mass spectrometer (Heinritzi et al., 2016). The calibrations of [SA] and transmission efficiency were performed before each campaign. A Vocus proton-transferreaction time-of-flight mass spectrometer (Vocus PTR-ToF-MS, Aerodyne Research Inc.) equipped with a focusing ionmolecular reactor (FIMR) was used at WD and DL, with modified instrument settings to measure DMA (Wang et al., 2020). A chemical ionization high-resolution time-of-flight mass spectrometer (CI-HToF-MS, Aerodyne Research Inc.) was used at TL, with protonated ethanol or its hydrated clusters as reagent ions, to measure DMA (Yao et al., 2016). Since mass spectrometer cannot distinguish among isomers, C₂-amine was taken as DMA. NH₃ concentration ([NH₃]) was measured using the ion chromatography (IC) method of Chinese Standard (HJ 1076-2019) at WD and DL. There was no measurement for [NH₃] at TL. The detailed measurement methods for these chemical species are given in the Supplement.

PSD ranging from 1 to 3 nm was measured by an Airmodus A10 particle size magnifier (PSM). The PSD of 3–736 nm particles was measured by two scanning mobility particle sizers (SMPS TSI Inc, USA), namely a nano-SMPS and a long-SMPS (Yao et al., 2018). Temperature was monitored by an automatic weather station (Vaisala AWS310).

2.2 Models

A cluster dynamics-multicomponent sectional model was applied to simulate SA-DMA nucleation process (Li et al., 2023). The model is composed of one cluster dynamics module and one sectional module. The detailed description of these two modules is given in the Supplement. SA tetramers were treated as nucleated particles for simulating particle formation rate at 1.4 nm diameter, $J_{1.4}$ (Larriba et al., 2011), and entered the sectional module as the smallest particles. Particle formation rate at 1.7 nm diameter, $J_{1.7}$, was simulated by incorporating the initial growth on the basis of $J_{1.4}$. How-

ever, in certain cases, this process could not be directly implemented in the model, because of data overflow (Fig. S2). Therefore, a survival probability approach was adopted as an alternative (Cai et al., 2022a):

$$\frac{J_{p_1}(t)}{J_{p_2}(t)} = \exp \int_{d_{p_2}}^{d_{p_1}} -\frac{\text{CoagS}(d_p)}{\text{GR}(d_p)} dd_p$$
 (1)

where $d_{\rm p1}$ is 1.7 nm, and $d_{\rm p2}$ is 1.4 nm, the corresponding particle size in calculating particle formation rates. The ratio $J_{1.4}/J_{1.7}$ is defined as the survival probability from 1.4 to 1.7 nm. GR is herein the simulated size-dependent growth rate, which is contributed by condensable vapors through the change of particle mass over time (Tröstl et al., 2016):

$$\frac{\mathrm{d}m_{\mathrm{p}}}{\mathrm{d}t} = \sum_{i} m_{i} \left(\alpha \beta_{i} N_{i} - \beta_{i} N_{i},_{\mathrm{sat}} \exp \left(\frac{4 v_{i} \sigma}{d_{\mathrm{p}} k_{\mathrm{B}} T} \right) f_{i} \right) \tag{2}$$

where m_p is the mass of particle; i represents each condensable species; m_i is the mass of molecules or clusters; α is the accommodation coefficient; β_i is the collision constant between species i and the particle; $N_{i,sat}$ is the saturation concentration; v_i is the molecular volume; σ is the surface tension of the particle; k_B is the Boltzmann constant; f_i is the molar fraction in the particle. In calculations, the fragmentation of SA-DMA clusters from particles was taken to be negligible, i.e., clusters did not return to the gas phase after coagulating onto a particle.

2.3 Uncertainty analysis

The uncertainty of SA monomer concentration ($[SA_1]$) was estimated to be +100 % / -50 % (Cai et al., 2021). The uncertainty of [DMA] was +150%/-60% taking into account systematic and calibration uncertainties among campaigns (Freshour et al., 2014). The uncertainty of [OOMs] was expected to be greater than that of $[SA_1]$, because it was quantified by the calibration factor of SA. Li et al. (2023) reported that [OOMs] with a scaling factor of 1.35-4 could explain the measured new particle growth. Hence, the uncertainty of OOMs was estimated to be +200% / -66%. In terms of the volatility estimation of OOMs, the logarithm of saturation mass concentration (logC*) had an uncertainty of ± 1 (Stolzenburg et al., 2018). The uncertainties of CS and measured particle formation rate were $\pm 10\%$ and +100% / -50%, respectively (Cai et al., 2021). All uncertainties of these parameters are listed in Table S1.

The uncertainties of simulated values, like the SA dimer concentration ([SA₂]) and the particle formation rate, were obtained by inputting the uncertainty ranges of measured data into the model. For example, the measured value of [SA₁], [DMA] and CS were scaled by factors of 2, 2.5, and 1.1 (according to their uncertainty) were input to calculate the upper boundary of the uncertainty range of simulated [SA₂] ([SA₂]_{sim}) and simulated $J_{1.4}$ ($J_{1.4,sim}$) and the lower boundary of simulated value was calculated in a similar way

Site	Location	Period	Instrument					
			SA & OOMs	DMA	NH ₃	PSD		
WD	38°39′ N, 115°11′ E	Dec 2018–Jan 2019		Vocus	IC			
DL	31°05′ N, 120°59′ E	Dec 2022–Jan 2023 & Apr 2023–Jun 2023	CI-LToF-MS	PTR-ToF -MS		nano-SMPS+ long-SMPS		
TL	31°25′ N, 120°13′ E	Jul 2023–Sep 2023	-	CI-HToF -CIMS	Not available	+ PSM		

Table 1. The location, period and the usage of instrument at different sites.

to the upper boundary, except that scale factors of 2, 2.5 and 1.1 were replaced by 0.5, 0.4 and 0.9, respectively.

2.4 Scaling processing

To quantitatively characterize the effects of $[SA_1]$ and temperature on $[SA_2]$ and particle formation rate, we normalized the effects of CS and [DMA] by scaling the measured values to consistent conditions based on simulation. Here, the scaling of measured $[SA_2]$ ($[SA_2]_{meas}$) is defined as follows:

$$[SA2]scaled = [SA2]meas \cdot C(CSmedian, [DMA]median)$$
(3)

where $[SA_2]_{scaled}$ refers to the scaled $[SA_2]_{meas}$; $C(CS_{median}, [DMA]_{median})$ is the scaling coefficient for $[SA_2]_{meas}$ and was calculated by:

$$C(CS_{median}, [DMA]_{median}) = \frac{[SA_2]_{sim, median}}{[SA_2]_{sim}}$$
(4)

where $[SA_2]_{sim}$ denotes the simulated SA_2 concentration calculated by inputting measured $[SA_1]$, [DMA], CS and temperature into the cluster dynamics-multicomponent sectional model; $[SA_2]_{sim,median}$ was calculated using measured $[SA_1]$ and temperature, combined with the median [DMA] (2.3 pptv) and the median CS (0.017 s $^{-1}$) in all NPF events. $[SA_2]_{sim,median}$ is regarded as the theoretical $[SA_2]_{meas}$ when measured [DMA] and CS attain their event medians. [DMA] was unavailable at SH. Considering high [DMA] (0.7–54.3 pptv) in other campaigns in urban Shanghai (Yao et al., 2016; Chang et al., 2021), a fixed [DMA] (5 pptv) was set for scaling, almost reaching the nucleation limit under the atmospheric $[SA_1]$ (Almeida et al., 2013). The analogous scaling methodology for particle formation rates is detailed in the Supplement.

3 Results and discussion

3.1 SA-DMA nucleation for all the campaigns

SA and DMA can explain the atmospheric nucleation observed at all sites. This finding is supported by the correlation between $[SA_1]$ and particle formation rates, the composition of detected clusters, the alignment of simulated and

measured nucleation intensity ([SA₂] and particle formation rates), and the dependences of NPF on temperature and [DMA]. The first two points are addressed in this section, while the remaining evidence will be discussed in Sect. 3.2 and 3.3.

Figure 1 shows the measured particle formation rates at 1.7 nm diameter $(J_{1.7,\text{meas}})$ as a function of [SA₁] and compares them with those in other studies. All measured particle formation rates are much higher than SA-NH₃ at corresponding temperatures of Cosmics Leaving Outdoor Droplets (CLOUD) experiments, which suggests the existence of precursors with higher basicity, like amines (Kirkby et al., 2011; Almeida et al., 2013). Our data (except TL) are in accordance with SA-DMA-NH₃(-OOMs) nucleation at 293 K of CLOUD, even though the median temperature in our campaigns was 287 K. Data from TL follow the simulated line for SA-DMA nucleation at 303 K. Furthermore, our observed results align closely with those at SH and BJ, where SA and DMA have been suggested to be key nucleating precursors (Yao et al., 2018; Cai et al., 2021), indicating a potentially consistent nucleation mechanism across these locations. Compared with CLOUD experimental conditions (Table 2), our campaigns exhibited higher CS and lower [DMA], both of which were unfavorable for NPF. This explains the generally lower particle formation rates observed in our measurements relative to those from CLOUD under varying temperature conditions. Therefore, the observed nucleation is likely driven by SA and enhanced by strong stabilizing precursors such as DMA. Other nucleation mechanisms are unlikely to dominate under these conditions.

The composition of the measured cluster provides further evidence for the involvement of DMA in the formation of SA clusters (Fig. 2). A number of neutral clusters, including SA and SA-DMA clusters, were observed at WD, DL and TL. These clusters are described as SA monomer (SA₁), dimer (SA₂), trimers (SA₃DMA₀₋₂) and tetramers (SA₄DMA₁₋₂), contributing to NPF. The absence of DMA in pure SA clusters can be attributed to in-situ fragmentation within the mass spectrometer (Alfaouri et al., 2022), suggesting more DMA molecules were expected to be existed in clusters. Similar patterns of SA-DMA clusters were also measured by CI-TOF-MS in other urban sites (Yao et al., 2018; Yin et

Data source		Temperature (K)	$\frac{\text{CS}}{(\text{s}^{-1})}$	[DMA] (pptv)	[OOMs] (cm ⁻³)	[NH ₃] (ppbv)
This study	median range	290 268–307	0.017 0.008–0.060	2.3 0.6–18.3	$1.8 \times 10^8 2.0 \times 10^7 - 9.7 \times 10^8$	2.1 0.4–7
CLOUD (Xiao Shanghai (Yao o Beijing (Cai Qiao et al., 202	et al., 2018) et al., 2021;	278, 293 267–291 275–289	0.002–0.008 0.017–0.039 0.005–0.021	4 not available 0.7–3.5	up to 8.8×10^9 $2.3 \times 10^7 - 2.1 \times 10^8$ $1.2 \times 10^7 - 6.4 \times 10^7$	1–2.5 not available 0.3–2.3

Table 2. Comparison of NPF characteristics in different campaigns.

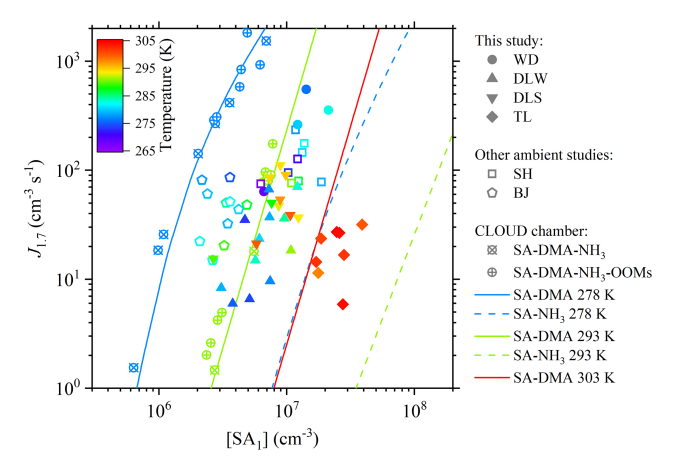


Figure 1. $J_{1.7,meas}$ as a function of [SA₁] with the comparison of ambient data and CLOUD. Rainbow filled symbols represent measured data, and each symbol indicates one NPF event with the time resolution of 30 min, which were selected when $J_{1.7,meas}$ reaches maximum. Rainbow open symbols represent data from published studies (Yao et al., 2018; Cai et al., 2021). Symbols with crosses indicate CLOUD data in the temperature of 278 and 293 K, respectively. Lines represent the fitting result of CLOUD (Xiao et al., 2021), except for the SA-DMA fitting at 303 K that is derived from the CLOUD fitting line of SA+DMA 293 K by the cluster dynamics-multicomponent sectional model.

al., 2021). Besides, the normalized signal of SA trimer and tetramer show good correlations ($r^2 = 0.44$ –0.76) with the number concentration of particles below 3 nm (Fig. S3). Such correlations between clusters and newly formed particles were reported in other atmospheric observations (Bianchi et al., 2016; Yan et al., 2021), indicating that these clusters typically signified the molecular clustering processes in NPF events. Other molecules that may participate in nucleation, such as OOMs and NH₃, were not detected in clusters, as they are generally in the form of ion clusters rather than neutral clusters (Bianchi et al., 2016; Yin et al., 2021; Cai et al., 2024).

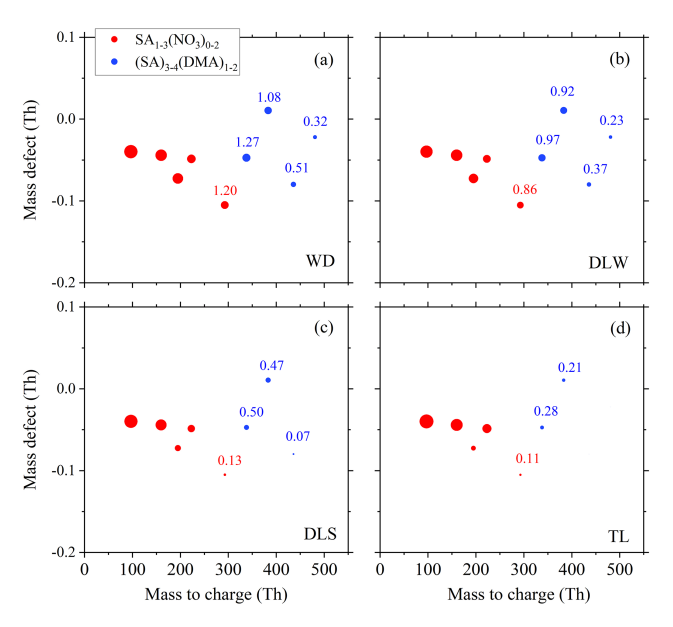


Figure 2. The mass defect of SA molecules and its clusters during four NPF events on (a) 20 January 2019 at WD (temperature = 275 K; $[SA_1] = 1.4 \times 10^7 \, \text{cm}^{-3}$; $CS = 0.055 \, \text{s}^{-1}$; $[DMA] = 3.4 \, \text{pptv}$); (b) 27 January 2023 at DLW (temperature = 277 K; $[SA_1] = 7.3 \times 10^6 \, \text{cm}^{-3}$; $CS = 0.012 \, \text{s}^{-1}$; $[DMA] = 1.5 \, \text{pptv}$); (c) 2 May 2023 at DLS (temperature = 295 K; $[SA_1] = 9.5 \times 10^6 \, \text{cm}^{-3}$; $CS = 0.014 \, \text{s}^{-1}$; $[DMA] = 2.9 \, \text{pptv}$); (d) 7 August 2023 at TL (temperature = 304 K; $[SA_1] = 2.6 \times 10^7 \, \text{cm}^{-3}$; $CS = 0.023 \, \text{s}^{-1}$; $[DMA] = 1.8 \, \text{pptv}$). Other species detected by CI-LToF-MS were not shown, because they are not expected to participate in atmospheric nucleation. The area of symbol is proportional to the logarithm of normalized signal. (multiplied by a factor of $1 \times 10^6 \, \text{before}$ taking the logarithm). The logarithm of values is annotated for some larger clusters.

3.2 The influencing factors of NPF

We analyzed the factors determining the occurrence of NPF events in different campaigns by contrasting NPF and non-NPF events (Fig. 3). [SA₁] during NPF periods was 0.5–2 times higher than that during non-NPF periods at DL and TL, suggesting [SA₁] was key to determining the occurrence of NPF at these sites (Fig. 3a). This pattern resembles that

observed in Barcelona (Brean et al., 2020) but differs from that observed in Beijing (Deng et al., 2020; Yan et al., 2021), where low CS was related to the occurrence of NPF without evident variations in [SA₁]. CS during NPF periods was generally lower than that during non-NPF periods in all campaigns, except DLS, further confirming that high preexisting aerosols suppressed the occurrence of NPF (Fig. 3b). However, NPF events were not significantly dependent on the CS in Po Valley, indicating other influencing factors govern the occurrence of NPF in less polluted atmospheres (Cai et al., 2024). Therefore, both the strength of precursor sources and pre-existing sink were important to the occurrence of NPF at our sites.

Besides SA, other potential precursors related to NPF in polluted regions including DMA, NH₃ and OOMs (Fig. S4). These species are known to enhance SA-driven nucleation (Kirkby et al., 2011; Almeida et al., 2013; Riccobono et al., 2014) and promote particle growth (Tröstl et al., 2016). Increasing [DMA] considerably enhances SA2 formation under fixed temperature ranges (Fig. S5), and this effect diminishes as [DMA] approaches nucleation saturation (Almeida et al., 2013). This phenomenon supports the contribution of DMA to atmospheric nucleation and is consistent with the results from a flow reactor (Jen et al., 2014). Moreover, it is likely that OOMs and NH₃ played a synergistic role in nucleation under our campaign conditions. Multiple studies have detected clusters containing these precursors, such as SA-DMA-NH₃, SA-NH₃-OOMs, SA-NH₃ and SA-OOMs, in the presence of DMA in polluted atmospheres, and some of these clusters showed positive correlations with particles below 3 nm (Yan et al., 2021; Yin et al., 2021; Cai et al., 2024). In CLOUD studies, the contributions of OOMs and NH₃ to cluster formation were not as considerable as that of DMA (Kürten et al., 2018; Xiao et al., 2021). Given that our field measurements exhibited similar [NH₃] and relatively low [OOMs] compared to those in CLOUD experiments (Table 2), it follows that their effects were unlikely to be greater than DMA in our campaigns. Despite the potential participation of other precursors, the observation-simulation agreement suggests DMA is a major base that stabilizes SA clusters (Fig. S5). However, [DMA] and [NH₃] were not markedly elevated during NPF periods (Fig. S4). The likely reason is that the suppression of NPF by high CS masked the enhancing effect of DMA and NH3, as they were positively correlated with CS ($r^2 = 0.31$ and 0.39, respectively, Fig. S6).

Although the occurrence of NPF is not strongly dependent on ambient temperature in individual campaigns (Fig. 3c), the intercomparison across campaigns indicates a general negative correlation between NPF frequency and temperature, reflecting seasonal characteristics (Fig. 3d). This trend is consistent with long-term measurements in Chacaltaya (Rose et al., 2015), Beijing (Deng et al., 2020) and Gwangju (Lee et al., 2024), where NPF was most frequent in winter and least frequent in summer. The intercomparison of cam-

paigns further shows that temperature played a key role in determining the intensity of NPF indicated by [SA₂] and $J_{1.7,meas}$ (Fig. 3e–f). Temperature even exerted more dominant influence than [SA₁] and CS. For example, despite the highest [SA₁] at TL, its elevated temperatures (298–306 K) resulted in lower median values of [SA₂] and $J_{1.7,meas}$ than those in all campaigns. Conversely, WD had the lowest temperature (281–268 K) and relatively high [SA₁] (7 × 10^6 – 1.8×10^7 cm⁻³), the intensity of NPF at WD was the highest, even under strong coagulation scavenging (median CS = ~ 0.05 s⁻¹). A more detailed discussion regarding the influence of temperature on NPF is provided in Sect. 3.3.

3.3 The dependence of nucleation on temperature

Figure 4 shows that [SA₂]_{meas} is in accordance with [SA₂]_{sim} when considering the uncertainties. It means DMA, as a major stabilizer, can sufficiently explain the formation of SA₂. In addition to DMA, other gases could have participated in stabilizing SA₂. Kirby et al. (2011) reported the detection of SA₂ in the SA-NH₃ system of CLOUD experiments. Jen et al. (2014) found that methylamine (MA) and trimethylamine (TMA) contributed to the formation of neutral SA₂. Riccobono et al. (2014) observed that OOMs were able to be bounded to ion SA₂. Furthermore, [SA₂]_{meas} is slightly lower than [SA₂]_{sim} overall. Similar discrepancies between measured and simulated cluster concentrations have also been reported in CLOUD experiments (Kürten et al., 2014). This systematic underestimation is likely attributable to measurement errors, because not all SA2 is fully detected, as some may dissociate within the mass spectrometer (Alfaouri et al., 2022). The observation-simulation comparison of $J_{1.4}$ is shown in Fig. S7, where simulation results fall within acceptable ranges upon uncertainty analysis. The consistency between measured and simulated parameters ([SA₂] and $J_{1.4}$) supports the significance of SA-DMA collision in NPF.

The consistency between measured and simulated parameters also validates the applicability of the model for data scaling. After accounting for the influences of CS and [DMA], [SA₂]_{scaled} exhibits a significant decreasing trend with rising temperature, showing agreement with simulated results (Fig. 5). This trend underscores the effect of temperature in governing the stability and abundance of clusters in nucleation pathways. At the molecular level, it is proposed that SA and DMA form SA₁DMA₁ clusters, which subsequently contributes to SA2 formation, during nucleation (Olenius et al., 2017; Myllys et al., 2019). Compared with $SA_2(DMA)_{1-2}$, SA_1DMA_1 is more sensitive to temperature (Cai et al., 2022b). Thus, in addition to the evaporation of SA dimer, SA₁DMA₁ formation also acts as a rate-limiting step in clustering. Kürten et al. (2016) and Brean et al. (2020) observed relatively low ratios of $[SA_2]$ to $[SA_1]$ (~ 0.01) at an urban site and a rural site, respectively, and speculated that they were related to higher temperatures (298–308 K).

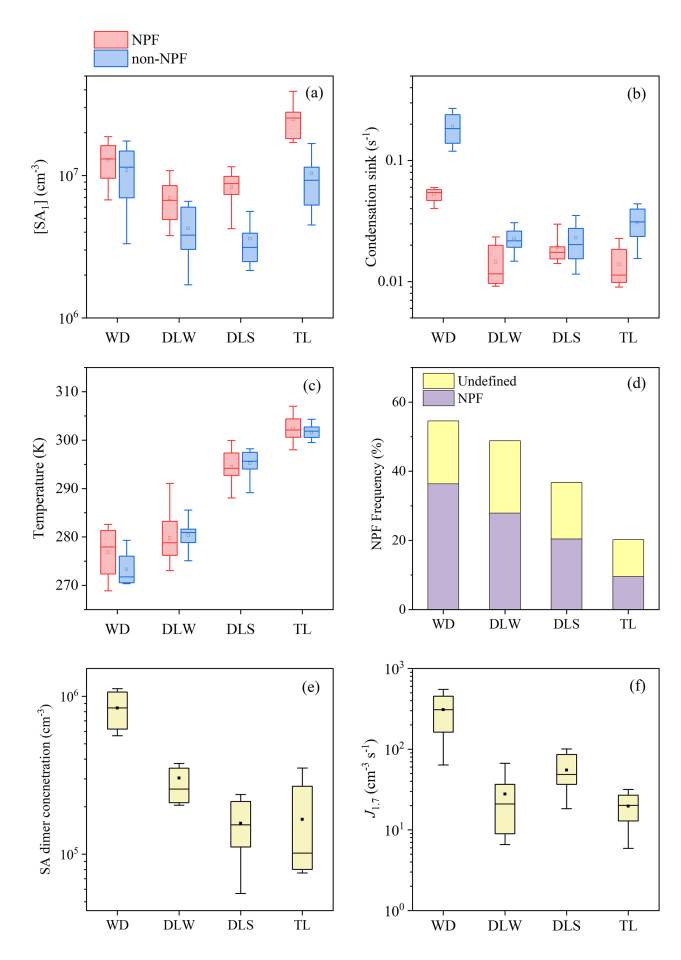


Figure 3. Parameters related to NPF. (a) $[SA_1]$, (b) CS, (c) temperature during NPF periods and non-NPF periods, (d) NPF frequency in each campaign, and (e) $[SA_2]$ and (f) $J_{1.7,meas}$ during NPF periods. The NPF period is defined as the period with the maximum value of $J_{1.7}$ in each NPF event, and the non-NPF period is defined as the median range of all NPF periods (09:00–11:00 LT) in non-NPF days. In order to eliminate the influence of precipitation, only sunny and cloudy days are selected for non-NPF. The transverse lines and square markers inside the boxes indicate mean values and median values, respectively. The bottom and top edges of the box indicate the 25th and 75th percentiles, respectively. The bottom and top edges of the whisker lines outside of the boxes indicate the 10th and 90th percentiles, respectively.

An intercomparison of the panels in Fig. 2 shows that the abundance and variety of larger SA-DMA clusters (SA trimers and tetramers) decline with increasing temperature, despite variations in precursor concentrations and CS across sites. For instance, although TL exhibited higher [SA₁] ($\sim 2.6 \times 10^7 \, \rm cm^{-3}$) during high-temperature ($\sim 303 \, \rm K$) NPF periods, the abundance and diversity of measured clusters were lower than those at low-temperature sites (WD and DLW). The observed reduction in the abundance of larger clusters at elevated temperatures is constrained by smaller ones (SA monomers and dimers), since the evaporation rates of

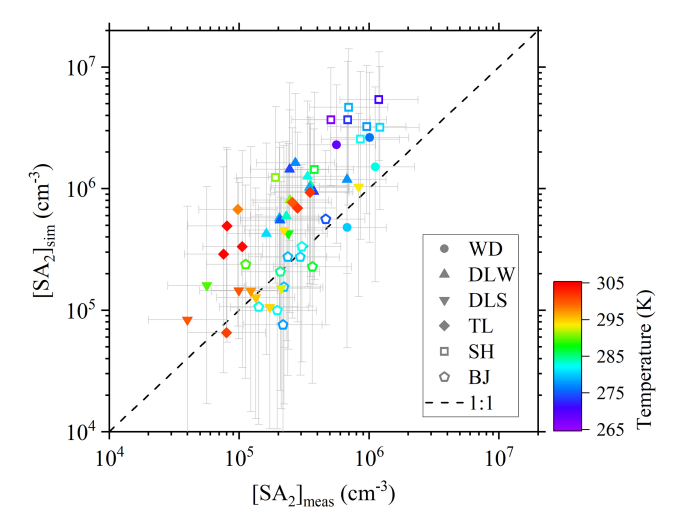


Figure 4. The comparison between $[SA_2]_{meas}$ and $[SA_2]_{sim}$. Horizontal and vertical error bars connected with each symbol indicate the uncertainties of x-axis and y-axis, respectively.

SA trimers and tetramers show relatively low sensitivity to temperature (Olenius et al., 2017). The proportion of base molecules in clusters also decreased with increasing temperature in the four selected NPF events, which was also reported in CLOUD experiments (Schobesberger et al., 2015). Furthermore, with the increase of cluster size, NH₃ tends to gradually replace DMA in ion clusters (Schobesberger et al., 2015; Yin et al., 2021), enhancing the stability of SA-base clusters (Bzdek et al., 2017), which helps them resist evaporation.

As shown in Fig. 6, the particle formation rate exhibits a negative correlation with temperature. Notably, for a fixed $[SA_1]$, the formation rate varies by approximately 3 orders of magnitude over a 30 K temperature range, and this extent of variation is comparable to that reported in chamber experiments simulating the conditions of polluted environments (Xiao et al., 2021) and atmospheric observations in urban area (Yu et al., 2016). This highlights the critical role of temperature in modulating nucleation, suggesting that temperature fluctuations alone can induce major variability in NPF without the change in the species and concentrations of nucleation precursors. In other words, SA and DMA can still explain the wide range of $J_{1.4, \text{scaled}}$ at these sites.

In the analyses presented above, temperature is regarded as a dominant factor determining the intensity of NPF over large regional scales. The direct effect of temperature on NPF is negative, through altering the evaporation rates of clusters (Olenius et al., 2017; Myllys et al., 2019). This has been consistently demonstrated in well-controlled chamber experiments with different nucleation mechanisms (Kirkby et al., 2011; Simon et al., 2020; Xiao et al., 2021; He et al., 2023). When temperature differences are substantial, its inhibitory effect on NPF becomes evident in complex ambient environments. For example, Baalbaki et al. (2021) reported

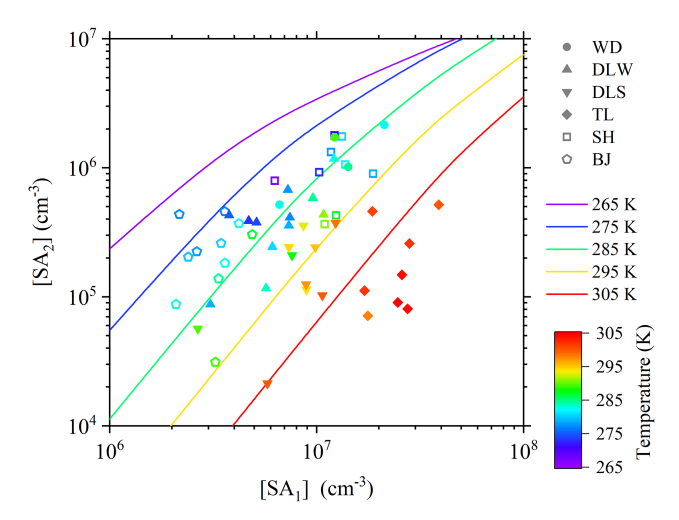


Figure 5. [SA₂]_{scaled} as a function of [SA₁] under a temperature gradient. Each symbol indicates one NPF event with a time resolution of 30 min, which was selected when $J_{1.7,meas}$ reaches maximum. [DMA] and CS for the simulated lines calculated by the discrete-sectional model are their median values in all NPF events, i.e., $0.017 \, \mathrm{s}^{-1}$ and $2.3 \, \mathrm{pptv}$, respectively. To visualize the effect of temperature, the color of the simulated lines corresponds to the color bar.

the particle formation rate in warmer months was actually lower than that in cooler months with comparable [SA₁] levels in the Eastern Mediterranean. Inter-site comparisons in India showed a negative correlation between particle formation rate and temperature, although precursor concentrations were not measured (Kanawade et al., 2022). However, under conditions of limited temperature variability, the effect of temperature is less directly observable, and higher temperatures may even appear to favor NPF (Größ et al., 2018; Brean et al., 2020; Yan et al., 2021; Victor et al., 2024). This may stem from other temperature-related factors. For example, in atmospheric observations, temperature is often correlated positively with solar radiation, which directly promotes the formation of nucleation precursors (Kürten et al., 2016; Brean et al., 2020). Additionally, temperature is typically negatively correlated with relative humidity, and high humidity suppresses NPF via hygroscopic growth of pre-existing particles (Määttänen et al., 2018).

3.4 Initial growth of nucleated particles

The analyze above has shown that SA and DMA can explain atmospheric nucleation. Here, the initial growth of nucleated particles is investigated. Figure 7a compares the simulated growth rate of 1.4–1.7 nm particles (GR_{1.4–1.7}) with two sets of condensable vapors at BJ and DLS. When only SA and its clusters are included, the simulated GR_{1.4–1.7} ranges approximately from 0.3 to 3.4 nm h⁻¹. The simulated GR_{1.4–1.7} is enhanced when OOMs are also considered as condensable vapors on the basis of the contribution of SA and its clus-

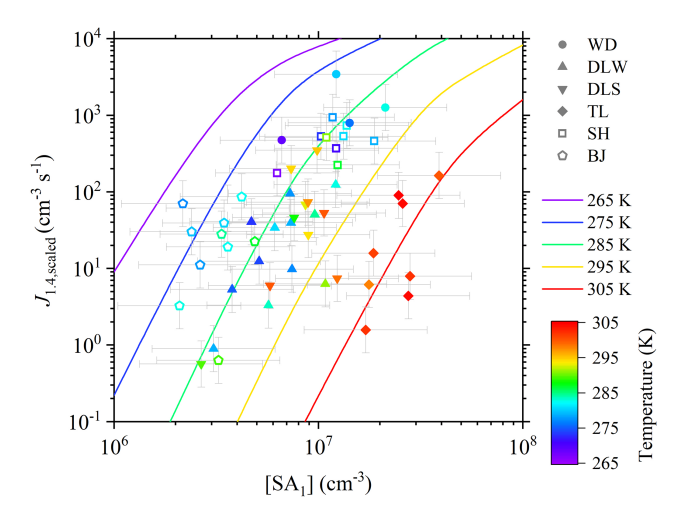


Figure 6. $J_{1.4, \text{scaled}}$ as a function of [SA₁] under the temperature gradient. Each symbol indicates one NPF event with a time resolution of 30 min, which was selected when $J_{1.7, \text{meas}}$ reaches maximum. [DMA] and CS for the simulated lines by the discrete-sectional model are their median values in all NPF events, i.e., $0.017 \, \text{s}^{-1}$ and $2.3 \, \text{pptv}$, respectively. Horizontal and vertical error bars connected with each symbol indicate the uncertainties of x-axis and y-axis, respectively. To visualize the effect of temperature, the color of the simulated lines corresponds to the color bar.

ters, ranging approximately from 1.2 to $22.6 \,\mathrm{nm}\,\mathrm{h}^{-1}$. Assuming $\mathrm{GR}_{1.4-1.7}$ is roughly approximated to the growth rate of particles below 3 nm, these simulated values are generally in accordance with the measured range $(0.5-20.4 \,\mathrm{nm}\,\mathrm{h}^{-1})$ in previous reports from the eastern region of China (Xiao et al., 2015; Dai et al., 2017; Yao et al., 2018; Hong et al., 2023). The corresponding simulation results from the other four campaigns are generally consistent with those at BJ and DLS, differing mainly in the extent of growth rate enhancement (Fig. S8a).

The comparison between $J_{1.7,\text{meas}}$ and simulated $J_{1.7}$ $(J_{1.7,\text{sim}})$ provides support for the contribution of OOMs to the growth of nucleated particles (Fig. 7b). When only SA and its clusters are considered, a substantial deviation, sometimes more than 3 orders of magnitude, is observed between $J_{1.7,\text{meas}}$ and $J_{1.7,\text{sim}}$. Compared to the simulation of $J_{1.4}$ (Fig. S7), $J_{1.7,\text{sim}}$ shows a noticeable decline at DLS and BJ. The inclusion of OOM-induced growth markedly increases $J_{1.7.\text{sim}}$, leading to better agreements with measurements, which can also be supported by observations in CLOUD experiments (Tröstl et al., 2016). The corresponding improvement are limited at WD, DLW, TL and SH, where the contribution of SA and its clusters seems sufficient to explain GR_{1,4-1,7} (Fig. S8b). In fact, some ultralow volatile organic compounds within OOMs may be involved in nucleating (Simon et al., 2020). Nevertheless, even without considering their contribution in this stage, the condensation of OOMs exerts a considerable influence on initial growth, as reflected

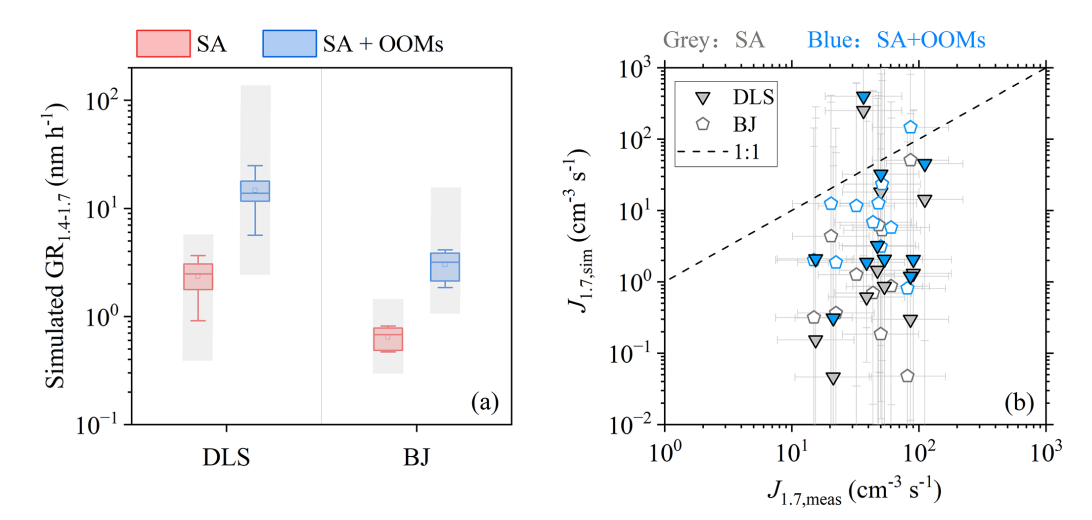


Figure 7. The simulation of $GR_{1.4-1.7}$ and $J_{1.7}$. (a) The comparison of simulated $GR_{1.4-1.7}$ contributed by SA and its clusters (i.e. SA in the legend), as well as SA and its clusters plus OOMs in campaigns. The transverse lines and square markers inside the boxes indicate mean values and median values, respectively. The bottom and top edges of the box indicate the 25th and 75th percentiles, respectively. The bottom and top edges of the whisker lines outside of the boxes indicate the 10th and 90th percentiles, respectively. The shade boxes indicate the ranges of uncertainties. (b) The comparison between $J_{1.7,\text{meas}}$ and $J_{1.7,\text{sim}}$. Horizontal and vertical error bars connected with each symbol indicate the uncertainties of x-axis and y-axis, respectively.

in $J_{1.7}$. Moreover, $J_{1.7}$ exhibits strong temperature dependence, similar to $J_{1.4}$ (Fig. S9).

4 Conclusions

We studied the mechanism and influencing factors of NPF on a large spatial scale by using observational data at multiple sites in the eastern region of China, including the concentrations of key chemical species, temperature and PSD.

By Comparing with previous studies that investigated atmospheric nucleation mechanism in individual sites, we have showed the applicability of a similar mechanism over a large geographic region. Based on the correlation between [SA₁] and particle formation rate, the identification of key clusters, and comparisons between simulations and measurements, we concluded that nucleating processes, mainly exemplified by SA_2 and $J_{1.4}$, could be largely attributed to SA-DMA collision. Other precursors, such as NH₃ and OOMs, might also have participated, since their concentrations were considerable and theoretically adequate to support nucleation. However, SA and its clusters were insufficient, at least at DSL and BJ, to explain the initial growth of nucleated particles, while OOMs make a great contribution to this process, thereby affecting $J_{1.7}$, which was derived from model-observation comparisons. While previous understanding of the contribution of OOMs to initial particle growth was reflected by chamber studies, our study provides supporting evidence from atmospheric observations. Given the considerable spatial separation among five sites, we infer that within this extensive urban agglomeration, SA and DMA are capable of describing atmospheric nucleation up to 1.4 nm, whereas OOMs are potentially involved in subsequent growth. This may also apply to other populated and polluted regions, where the NPF mechanism warrants investigation.

As for influencing factors, the occurrence of NPF was governed by $[SA_1]$ and CS, whereas the frequency and intensity of NPF were mainly determined by temperature, which generally exhibited a negative correlation with NPF over a wide temperature range. Compared with previous studies investigating NPF dependence on temperature from a temporal perspective, dependences of cluster concentrations and particle formation rates on temperature were illustrated quantitatively through scaling at five sites, suggesting the differences in nucleation intensity across this region could be explained by variations in temperature under the comparable mechanism. We expect that this finding holds for similar polluted atmospheric environments on large spatial scales worldwide, particularly where significant temperature gradients exist.

The case for SA-DMA nucleation presented in this study remains indirect, as it relies on precursors, limited clusters and modeling rather than comprehensive identification of nucleation process. To better resolve atmospheric nucleation mechanisms, future studies are warranted to advance beyond current methods of cluster detection, for instance, by enabling direct measurements of all basic molecules within SA clusters. In the complex urban atmosphere, the potential involvement of other pollutants will require novel direct measurements and analytical techniques, along with more comprehensive modeling, to clarify the roles of additional precursors.

Data availability. Data used in this work are available upon request from the corresponding authors.

Supplement. The supplement related to this article is available online at https://doi.org/10.5194/acp-25-17125-2025-supplement.

Author contributions. LW, JiaJ, RC designed the study. JiaJ, YiL, GY, YuL, CL, LY conducted the field campaigns. JinJ and XZ provided data and technical supports, respectively. JiaJ analyzed the data. JiaJ, RC and LW wrote the paper with contributions from all of the other co-authors.

Competing interests. The contact author has declared that none of the authors has any competing interests.

Disclaimer. Publisher's note: Copernicus Publications remains neutral with regard to jurisdictional claims made in the text, published maps, institutional affiliations, or any other geographical representation in this paper. While Copernicus Publications makes every effort to include appropriate place names, the final responsibility lies with the authors. Views expressed in the text are those of the authors and do not necessarily reflect the views of the publisher.

Acknowledgements. The authors would like to extend their gratitude to Chenxi Li from Shanghai Jiao Tong University for his assistance with coding.

Financial support. This work was supported by the National Key Research and Development Program of China (grant no. 2022YFC3704100) and the National Natural Science Foundation of China (grant nos. 22127811 and 21925601).

Review statement. This paper was edited by Ari Laaksonen and reviewed by two anonymous referees.

References

- Alfaouri, D., Passananti, M., Zanca, T., Ahonen, L., Kangasluoma, J., Kubečka, J., Myllys, N., and Vehkamäki, H.: A study on the fragmentation of sulfuric acid and dimethylamine clusters inside an atmospheric pressure interface time-of-flight mass spectrometer, Atmos. Meas. Tech., 15, 11–19, https://doi.org/10.5194/amt-15-11-2022, 2022.
- Almeida, J., Schobesberger, S., Kürten, A., Ortega, I. K., Kupiainen-Määttä, O., Praplan, A. P., Adamov, A., Amorim, A., Bianchi, F., Breitenlechner, M., David, A., Dommen, J., Donahue, N. M., Downard, A., Dunne, E., Duplissy, J., Ehrhart, S., Flagan, R. C., Franchin, A., Guida, R., Hakala, J., Hansel, A., Heinritzi, M., Henschel, H., Jokinen, T., Junninen, H., Kajos, M., Kangasluoma, J., Keskinen, H., Kupc, A., Kurtén, T., Kvashin,

- A. N., Laaksonen, A., Lehtipalo, K., Leiminger, M., Leppä, J., Loukonen, V., Makhmutov, V., Mathot, S., McGrath, M. J., Nieminen, T., Olenius, T., Onnela, A., Petäjä, T., Riccobono, F., Riipinen, I., Rissanen, M., Rondo, L., Ruuskanen, T., Santos, F. D., Sarnela, N., Schallhart, S., Schnitzhofer, R., Seinfeld, J. H., Simon, M., Sipilä, M., Stozhkov, Y., Stratmann, F., Tomé, A., Tröstl, J., Tsagkogeorgas, G., Vaattovaara, P., Viisanen, Y., Virtanen, A., Vrtala, A., Wagner, P. E., Weingartner, E., Wex, H., Williamson, C., Wimmer, D., Ye, P., Yli-Juuti, T., Carslaw, K. S., Kulmala, M., Curtius, J., Baltensperger, U., Worsnop, D. R., Vehkamaki, H., and Kirkby, J.: Molecular understanding of sulphuric acid-amine particle nucleation in the atmosphere, Nature, 502, 359–363, https://doi.org/10.1038/nature12663, 2013.
- Baalbaki, R., Pikridas, M., Jokinen, T., Laurila, T., Dada, L., Bezantakos, S., Ahonen, L., Neitola, K., Maisser, A., Bimenyimana, E., Christodoulou, A., Unga, F., Savvides, C., Lehtipalo, K., Kangasluoma, J., Biskos, G., Petäjä, T., Kerminen, V.-M., Sciare, J., and Kulmala, M.: Towards understanding the characteristics of new particle formation in the Eastern Mediterranean, Atmos. Chem. Phys., 21, 9223–9251, https://doi.org/10.5194/acp-21-9223-2021, 2021.
- Bianchi, F., Tröstl, J., Junninen, H., Frege, C., Henne, S., Hoyle, C. R., Molteni, U., Herrmann, E., Adamov, A., Bukowiecki, N., Chen, X., Duplissy, J., Gysel, M., Hutterli, M., Kangasluoma, J., Kontkanen, J., Kürten, A., Manninen, H. E., Münch, S., Peräkylä, O., Petäjä, T., Rondo, L., Williamson, C., Weingartner, E., Curtius, J., Worsnop, D. R., Kulmala, M., Dommen, J., and Baltensperger, U.: New particle formation in the free troposphere: A question of chemistry and timing, Science, 352, 1109–1112, https://doi.org/10.1126/science.aad5456, 2016.
- Bousiotis, D., Pope, F. D., Beddows, D. C. S., Dall'Osto, M., Massling, A., Nøjgaard, J. K., Nordstrøm, C., Niemi, J. V., Portin, H., Petäjä, T., Perez, N., Alastuey, A., Querol, X., Kouvarakis, G., Mihalopoulos, N., Vratolis, S., Eleftheriadis, K., Wiedensohler, A., Weinhold, K., Merkel, M., Tuch, T., and Harrison, R. M.: A phenomenology of new particle formation (NPF) at 13 European sites, Atmos. Chem. Phys., 21, 11905–11925, https://doi.org/10.5194/acp-21-11905-2021, 2021.
- Brean, J., Beddows, D. C. S., Shi, Z., Temime-Roussel, B., Marchand, N., Querol, X., Alastuey, A., Minguillón, M. C., and Harrison, R. M.: Molecular insights into new particle formation in Barcelona, Spain, Atmos. Chem. Phys., 20, 10029–10045, https://doi.org/10.5194/acp-20-10029-2020, 2020.
- Bzdek, B. R., DePalma, J. W., and Johnston, M. V.: Mechanisms of atmospherically relevant cluster growth, Acc. Chem. Res., 50, 1965–1975, https://doi.org/10.1021/acs.accounts.7b00213, 2017.
- Cai, J., Sulo, J., Gu, Y., Holm, S., Cai, R., Thomas, S., Neuberger, A., Mattsson, F., Paglione, M., Decesari, S., Rinaldi, M., Yin, R., Aliaga, D., Huang, W., Li, Y., Gramlich, Y., Ciarelli, G., Quéléver, L., Sarnela, N., Lehtipalo, K., Zannoni, N., Wu, C., Nie, W., Kangasluoma, J., Mohr, C., Kulmala, M., Zha, Q., Stolzenburg, D., and Bianchi, F.: Elucidating the mechanisms of atmospheric new particle formation in the highly polluted Po Valley, Italy, Atmos. Chem. Phys., 24, 2423–2441, https://doi.org/10.5194/acp-24-2423-2024, 2024.
- Cai, R., Yan, C., Yang, D., Yin, R., Lu, Y., Deng, C., Fu, Y., Ruan, J., Li, X., Kontkanen, J., Zhang, Q., Kangasluoma, J., Ma, Y., Hao, J., Worsnop, D. R., Bianchi, F., Paasonen, P., Ker-

- minen, V.-M., Liu, Y., Wang, L., Zheng, J., Kulmala, M., and Jiang, J.: Sulfuric acid–amine nucleation in urban Beijing, Atmos. Chem. Phys., 21, 2457–2468, https://doi.org/10.5194/acp-21-2457-2021, 2021.
- Cai, R., Deng, C., Stolzenburg, D., Li, C., Guo, J., Kerminen, V.-M., Jiang, J., Kulmala, M., and Kangasluoma, J.: Survival probability of new atmospheric particles: closure between theory and measurements from 1.4 to 100 nm, Atmos. Chem. Phys., 22, 14571– 14587, https://doi.org/10.5194/acp-22-14571-2022, 2022.
- Cai, R., Yin, R., Yan, C., Yang, D., Deng, C., Dada, L., Kangasluoma, J., Kontkanen, J., Halonen, R., Ma, Y., Zhang, X., Paasonen, P., Petäjä, T., Kerminen, V.-M., Liu, Y., Bianchi, F., Zheng, J., Wang, L., Hao, J., Smith, J. N., Donahue, N. M., Kulmala, M., Worsnop, D. R., and Jiang, J.: The missing base molecules in atmospheric acid-base nucleation, Natl. Sci. Rev., 9, nwac137, https://doi.org/10.1093/nsr/nwac137, 2022b.
- Chang, Y., Gao, Y., Lu, Y., Qiao, L., Kuang, Y., Cheng, K., Wu, Y., Lou, S., Jing, S., Wang, H., and Huang, C.: Discovery of a potent source of gaseous amines in urban China, Environ. Sci. Technol. Lett., 8, 725–731, https://doi.org/10.1021/acs.estlett.1c00229, 2021.
- Dai, L., Wang, H., Zhou, L., An, J., Tang, L., Lu, C., Yan, W., Liu, R., Kong, S., Chen, M., Lee, S., and Yu, H.: Regional and local new particle formation events observed in the Yangtze River Delta region, China, J. Geophys. Res.-Atmos., 122, 2389–2402, https://doi.org/10.1002/2016JD026030, 2017.
- Deng, C., Fu, Y., Dada, L., Yan, C., Cai, R., Yang, D., Zhou, Y., Yin, R., Lu, Y., Li, X., Qiao, X., Fan, X., Nie, W., Kontkanen, J., Kangasluoma, J., Chu, B., Ding, A., Kerminen, V.-M., Paasonen, P., Worsnop, D. R., Bianchi, F., Liu, Y., Zheng, J., Wang, L., Kulmala, M., and Jiang, J.: Seasonal characteristics of new particle formation and growth in urban Beijing, Environ. Sci. Technol., 54, 8547–8557, https://doi.org/10.1021/acs.est.0c00808, 2020.
- Dinoi, A., Gulli, D., Weinhold, K., Ammoscato, I., Calidonna, C. R., Wiedensohler, A., and Contini, D.: Characterization of ultrafine particles and the occurrence of new particle formation events in an urban and coastal site of the Mediterranean area, Atmos. Chem. Phys., 23, 2167–2181, https://doi.org/10.5194/acp-23-2167-2023, 2023.
- Freshour, N. A., Carlson, K. K., Melka, Y. A., Hinz, S., Panta, B., and Hanson, D. R.: Amine permeation sources characterized with acid neutralization and sensitivities of an amine mass spectrometer, Atmos. Meas. Tech., 7, 3611–3621, https://doi.org/10.5194/amt-7-3611-2014, 2014.
- Gordon, H., Kirkby, J., Baltensperger, U., Bianchi, F., Breitenlechner, M., Curtius, J., Dias, A., Dommen, J., Donahue, N. M., Dunne, E. M., Duplissy, J., Ehrhart, S., Flagan, R. C., Frege, C., Fuchs, C., Hansel, A., Hoyle, C. R., Kulmala, M., Kürten, A., Lehtipalo, K., Makhmutov, V., Molteni, U., Rissanen, M. P., Stozkhov, Y., Tröstl, J., Tsagkogeorgas, G., Wagner, R., Williamson, C., Wimmer, D., Winkler, P. M., Yan, C., and Carslaw, K. S.: Causes and importance of new particle formation in the present-day and preindustrial atmospheres, J. Geophys. Res.-Atmos., 122, 8739–8760, https://doi.org/10.1002/2017JD026844, 2017.
- Größ, J., Hamed, A., Sonntag, A., Spindler, G., Manninen, H. E., Nieminen, T., Kulmala, M., Hõrrak, U., Plass-Dülmer, C., Wiedensohler, A., and Birmili, W.: Atmospheric new particle formation at the research station Melpitz, Germany: connec-

- tion with gaseous precursors and meteorological parameters, Atmos. Chem. Phys., 18, 1835–1861, https://doi.org/10.5194/acp-18-1835-2018, 2018.
- Hanson, D. R., McMurry, P. H., Jiang, J., Tanner, D., and Huey, L. G.: Ambient pressure proton transfer mass spectrometry: detection of amines and ammonia, Environ. Sci. Technol., 45, 8881–8888, https://doi.org/10.1021/es201819a, 2011.
- He, X.-C., Simon, M., Iyer, S., Xie, H.-B., Rörup, B., Shen, J., Finkenzeller, H., Stolzenburg, D., Zhang, R., Baccarini, A., Tham, Y. J., Wang, M., Amanatidis, S., Piedehierro, A. A., Amorim, A., Baalbaki, R., Brasseur, Z., Caudillo, L., Chu, B., Dada, L., Duplissy, J., El Haddad, I., Flagan, R. C., Granzin, M., Hansel, A., Heinritzi, M., Hofbauer, V., Jokinen, T., Kemppainen, D., Kong, W., Krechmer, J., Kurt'en, A., Lamkaddam, H., Lopez, B., Ma, F., Mahfouz, N. G. A., Makhmutov, V., Manninen, H. E., Marie, G., Marten, R., Massabò, D., Mauldin, R. L., Mentler, B., Onnela, A., Petäjä, T., Pfeifer, J., Philippov, M., Ranjithkumar, A., Rissanen, M. P., Schobesberger, S., Scholz, W., Schulze, B., Surdu, M., Thakur, R. C., Tomé, A., Wagner, A. C., Wang, D., Wang, Y., Weber, S. K., Welti, A., Winkler, P. M., Zauner-Wieczorek, M., Baltensperger, U., Curtius, J., Kurtén, T., Worsnop, D. R., Volkamer, R., Lehtipalo, K., Kirkby, J., Donahue, N. M., Sipilä, M., and Kulmala, M.: Iodine oxoacids enhance nucleation of sulfuric acid particles in the atmosphere, Science, 382, 1308-1314 https://doi.org/10.1126/science.adh2526, 2023.
- Heinritzi, M., Simon, M., Steiner, G., Wagner, A. C., Kürten, A., Hansel, A., and Curtius, J.: Characterization of the massdependent transmission efficiency of a CIMS, Atmos. Meas. Tech., 9, 1449–1460, https://doi.org/10.5194/amt-9-1449-2016, 2016.
- Hong, J., Tang, M., Wang, Q., Ma, N., Zhu, S., Zhang, S., Pan, X., Xie, L., Li, G., Kuhn, U., Yan, C., Tao, J., Kuang, Y., He, Y., Xu, W., Cai, R., Zhou, Y., Wang, Z., Zhou, G., Yuan, B., Cheng, Y., and Su, H.: Measurement Report: Wintertime new particle formation in the rural area of the North China Plain influencing factors and possible formation mechanism, Atmos. Chem. Phys., 23, 5699–5713, https://doi.org/10.5194/acp-23-5699-2023, 2023.
- Jen, C. N., McMurry, P. H., and Hanson, D. R.: Stabilization of sulfuric acid dimers by ammonia, methylamine, dimethylamine, and trimethylamine, J. Geophys. Res.-Atmos, 119, 7502–7514, https://doi.org/10.1002/2014JD021592, 2014.
- Kanawade, V. P., Sebastian, M., Hooda, R. K., and Hyvärinen, A.-P.: Atmospheric new particle formation in India: Current understanding and knowledge gaps, Atmos. Environ., 270, 118894, https://doi.org/10.1016/j.atmosenv.2021.118894, 2022.
- Kerminen, V.-M., Chen, X., Vakkari, V., Petäjä, T., Kulmala, M., and Bianchi, F.: Atmospheric new particle formation and growth: review of field observations, Environ. Res. Lett., 13, 103003, https://doi.org/10.1088/1748-9326/aadf3c, 2018.
- Kirkby, J., Curtius, J., Almeida, J., Dunne, E., Duplissy, J., Ehrhart, S., Franchin, A., Gagné, S., Ickes, L., Kürten, A., Kupc, A., Metzger, A., Riccobono, F., Rondo, L., Schobesberger, S., Tsagkogeorgas, G., Wimmer, D., Amorim, A., Bianchi, F., Breitenlechner, M., David, A., Dommen, J., Downard, A., Ehn, M., Flagan, R. C., Haider, S., Hansel, A., Hauser, D., Jud, W., Junninen, H., Kreissl, F., Kvashin, A., Laaksonen, A., Lehtipalo, K., Lima, J., Lovejoy, E. R., Makhmutov, V., Mathot, S., Mikkilä, J.,

- Minginette, P., Mogo, S., Nieminen, T., Onnela, A., Pereira, P., Petäjä, T., Schnitzhofer, R., Seinfeld, J. H., Sipilä, M., Stozhkov, Y., Stratmann, F., Tomé, A., Vanhanen, J., Viisanen, Y., Vrtala, A., Wagner, P. E., Walther, H., Weingartner, E., Wex, H., Winkler, P. M., Carslaw, K. S., Worsnop, D. R., Baltensperger, U., and Kulmala, M.: Role of sulphuric acid, ammonia and galactic cosmic rays in atmospheric aerosol nucleation, Nature, 476, 429–433, https://doi.org/10.1038/nature10343, 2011.
- Kirkby, J., Amorim, A., Baltensperger, U., Carslaw, K. S., Christoudias, T., Curtius, J., Donahue, N. M., Haddad, I. E., Flagan, R. C., Gordon, H., Hansel, A., Harder, H., Junninen, H., Kulmala, M., Kürten, A., Laaksonen, A., Lehtipalo, K., Lelieveld, J., Möhler, O., Riipinen, I., Stratmann, F., Tomé, A., Virtanen, A., Volkamer, R., Winkler, P. M., and Worsnop, D. R.: Atmospheric new particle formation from the CERN CLOUD experiment, Nat. Geosci., 16, 948–957, https://doi.org/10.1038/s41561-023-01305-0, 2023.
- Kürten, A., Jokinen, T., Simon, M., Sipilä, M., Sarnela, N., Junninen, H., Adamov, A., Almeida, J., Amorim, A., Bianchi, F., Breitenlechner, M., Dommen, J., Donahue, N. M., Duplissy, J., Ehrhart, S., Flagan, R. C., Franchin, A., Hakala, J., Hansel, A., Heinritzi, M., Hutterli, M., Kangasluoma, J., Kirkby, J., Laaksonen, A., Lehtipalo, K., Leiminger, M., Makhmutov, V., Mathot, S., Onnela, A., Petäjä, T., Praplan, A. P., Riccobono, F., Rissanen, M. P., Rondo, L., Schobesberger, S., Seinfeld, J. H., Steiner, G., Tomé, A., Tröstl, J., Winkler, P. M., Williamson, C., Wimmer, D., Ye, P., Baltensperger, U., Carslaw, K. S., Kulmala, M., Worsnop, D. R., and Curtius, J.: Neutral molecular cluster formation of sulfuric acid—dimethylamine observed in real time under atmospheric conditions, Proc. Natl. Acad. Sci. U. S. A., 111, 15019–15024, https://doi.org/10.1073/pnas.1404853111, 2014.
- Kürten, A., Bergen, A., Heinritzi, M., Leiminger, M., Lorenz, V., Piel, F., Simon, M., Sitals, R., Wagner, A. C., and Curtius, J.: Observation of new particle formation and measurement of sulfuric acid, ammonia, amines and highly oxidized organic molecules at a rural site in central Germany, Atmos. Chem. Phys., 16, 12793–12813, https://doi.org/10.5194/acp-16-12793-2016, 2016.
- Kürten, A., Li, C., Bianchi, F., Curtius, J., Dias, A., Donahue, N. M., Duplissy, J., Flagan, R. C., Hakala, J., Jokinen, T., Kirkby, J., Kulmala, M., Laaksonen, A., Lehtipalo, K., Makhmutov, V., Onnela, A., Rissanen, M. P., Simon, M., Sipilä, M., Stozhkov, Y., Tröstl, J., Ye, P., and McMurry, P. H.: New particle formation in the sulfuric acid–dimethylamine–water system: reevaluation of CLOUD chamber measurements and comparison to an aerosol nucleation and growth model, Atmos. Chem. Phys., 18, 845–863, https://doi.org/10.5194/acp-18-845-2018, 2018.
- Larriba, C., Hogan Jr., C. J., Attoui, M., Borrajo, R., Garcia, J. F., and de la Mora, J. F.: The mobility-volume relationship below 3.0 nm examined by tandem mobilitymass measurement, Aerosol Sci. Tech., 45, 453–467, https://doi.org/10.1080/02786826.2010.546820, 2011.
- Lee, H., Cho, H., Yoon, Y. J., Kim, J., Lee, B. Y., and Park, K.: Comparison of new particle formation events in urban, agricultural, and arctic environments, Atmos. Environ., 333, 120634, https://doi.org/10.1016/j.atmosenv.2024.120634, 2024.
- Li, C., Li, Y., Li, X., Cai, R., Fan, Y., Qiao, X., Yin, R., Yan, C., Guo, Y., Liu, Y., Zheng, J., Kerminen, V.-M., Kulmala, M., Xiao, H., and Jiang, J.: Comprehensive simulations of new particle formation events in Beijing with a cluster dynamics—

- multicomponent sectional model, Atmos. Chem. Phys., 23, 6879–6896, https://doi.org/10.5194/acp-23-6879-2023, 2023.
- Lu, Y., Yan, C., Fu, Y., Chen, Y., Liu, Y., Yang, G., Wang, Y., Bianchi, F., Chu, B., Zhou, Y., Yin, R., Baalbaki, R., Garmash, O., Deng, C., Wang, W., Liu, Y., Petäjä, T., Kerminen, V.-M., Jiang, J., Kulmala, M., and Wang, L.: A proxy for atmospheric daytime gaseous sulfuric acid concentration in urban Beijing, Atmos. Chem. Phys., 19, 1971–1983, https://doi.org/10.5194/acp-19-1971-2019, 2019.
- Määttänen, A., Merikanto, J., Henschel, H., Duplissy, J., Makkonen, R., Ortega, I. K., and Vehkamäki, H.: New parameterizations for neutral and ion-induced sulfuric acid-water particle formation in nucleation and kinetic regimes, J. Geophys. Res.-Atmos., 123, 1269–1296, https://doi.org/10.1002/2017JD027429, 2018.
- Mohr, C., Thornton, J. A., Heitto, A., Lopez-Hilfiker, F. D., Lutz, A., Riipinen, I., Hong, J., Donahue, N. M., Hallquist, M., Petäjä, T., Kulmala, M., and Yli-Juuti, T.: Molecular identification of organic vapors driving atmospheric nanoparticle growth, Nat. Commun., 10, 4442, https://doi.org/10.1038/s41467-019-12473-2, 2019.
- Myllys, N., Kubečka, J., Besel, V., Alfaouri, D., Olenius, T., Smith, J. N., and Passananti, M.: Role of base strength, cluster structure and charge in sulfuric-acid-driven particle formation, Atmos. Chem. Phys., 19, 9753–9768, https://doi.org/10.5194/acp-19-9753-2019, 2019.
- Nieminen, T., Kerminen, V.-M., Petäjä, T., Aalto, P. P., Arshinov, M., Asmi, E., Baltensperger, U., Beddows, D. C. S., Beukes, J. P., Collins, D., Ding, A., Harrison, R. M., Henzing, B., Hooda, R., Hu, M., Hõrrak, U., Kivekäs, N., Komsaare, K., Krejci, R., Kristensson, A., Laakso, L., Laaksonen, A., Leaitch, W. R., Lihavainen, H., Mihalopoulos, N., Németh, Z., Nie, W., O'Dowd, C., Salma, I., Sellegri, K., Svenningsson, B., Swietlicki, E., Tunved, P., Ulevicius, V., Vakkari, V., Vana, M., Wiedensohler, A., Wu, Z., Virtanen, A., and Kulmala, M.: Global analysis of continental boundary layer new particle formation based on long-term measurements, Atmos. Chem. Phys., 18, 14737–14756, https://doi.org/10.5194/acp-18-14737-2018, 2018.
- Olenius, T., Halonen, R., Kurtén, T., Henschel, H., Kupiainen-Määtä, O., Ortega, I. K., Jen, C. N., Vehkamäki, H., and Riipinen, I.: New particle formation from sulfuric acid and amines: Comparison of monomethylamine, dimethylamine, and trimethylamine, J. Geophys. Res.-Atmos., 122, 7103–7118, https://doi.org/10.1002/2017JD026501, 2017.
- Qiao, X., Yan, C., Li, X., Guo, Y., Yin, R., Deng, C., Li, C., Nie, W., Wang, M., Cai, R., Huang, D., Wang, Z., Yao, L., Worsnop, D. R., Bianchi, F., Liu, Y., Donahue, N. M., Kulmala, M., and Jiang, J.: Contribution of atmospheric oxygenated organic compounds to particle growth in an urban environment, Environ. Sci. Technol., 55, 13646–13656, https://doi.org/10.1021/acs.est.1c02095, 2021.
- Riccobono, F., Schobesberger, S., Scott, C. E., Dommen, J., Ortega, I. K., Rondo, L., Almeida, J., Amorim, A., Bianchi, F., Breitenlechner, M., David, A., Downard, A., Dunne, E. M., Duplissy, J., Ehrhart, S., Flagan, R. C., Franchin, A., Hansel, A., Junninen, H., Kajos, M., Keskinen, H., Kupc, A., Kürten, A., Kvashin, A. N., Laaksonen, A., Lehtipalo, K., Makhmutov, V., Mathot, S., Nieminen, T., Onnela, A., Petäjä, T., Praplan, A. P., Santos, F. D., Schallhart, S., Seinfeld, J. H., Sipilä, M., Spracklen, D. V., Stozhkov, Y., Stratmann, F., Tomé, A., Tsagkogeorgas, G.,

- Vaattovaara, P., Viisanen, Y., Vrtala, A., Wagner, P. E., Weingartner, E., Wex, H., Wimmer, D., Carslaw, K. S., Curtius, J., Donahue, N. M., Kirkby, J., Kulmala, M., Worsnop, D. R., and Baltensperger, U.: Oxidation products of biogenic emissions contribute to nucleation of atmospheric particles, Science, 344, 717–721, https://doi.org/10.1126/science.1243527, 2014.
- Rose, C., Sellegri, K., Velarde, F., Moreno, I., Ramonet, M., Weinhold, K., Krejci, R., Ginot, P., Andrade, M., Wiedensohler, A., and Laj, P.: Frequent nucleation events at the high altitude station of Chacaltaya (5240 m a.s.l.), Bolivia, Atmos. Environ., 102, 18–29, https://doi.org/10.1016/j.atmosenv.2014.11.015, 2015.
- Schobesberger, S., Franchin, A., Bianchi, F., Rondo, L., Duplissy, J.,
 Kürten, A., Ortega, I. K., Metzger, A., Schnitzhofer, R., Almeida,
 J., Amorim, A., Dommen, J., Dunne, E. M., Ehn, M., Gagné, S.,
 Ickes, L., Junninen, H., Hansel, A., Kerminen, V.-M., Kirkby,
 J., Kupc, A., Laaksonen, A., Lehtipalo, K., Mathot, S., Onnela,
 A., Petäjä, T., Riccobono, F., Santos, F. D., Sipilä, M., Tomé,
 A., Tsagkogeorgas, G., Viisanen, Y., Wagner, P. E., Wimmer, D.,
 Curtius, J., Donahue, N. M., Baltensperger, U., Kulmala, M., and
 Worsnop, D. R.: On the composition of ammonia–sulfuric-acid
 ion clusters during aerosol particle formation, Atmos. Chem.
 Phys., 15, 55–78, https://doi.org/10.5194/acp-15-55-2015, 2015.
- Sebastian, M., Kanawade, V. P., and Pierce, J. R.: Observation of sub-3nm particles and new particle formation at an urban location in India, Atmos. Environ., 256, 118460, https://doi.org/10.1016/j.atmosenv.2021.118460, 2021.
- Simon, M., Dada, L., Heinritzi, M., Scholz, W., Stolzenburg, D., Fischer, L., Wagner, A. C., Kürten, A., Rörup, B., He, X.-C., Almeida, J., Baalbaki, R., Baccarini, A., Bauer, P. S., Beck, L., Bergen, A., Bianchi, F., Bräkling, S., Brilke, S., Caudillo, L., Chen, D., Chu, B., Dias, A., Draper, D. C., Duplissy, J., El-Haddad, I., Finkenzeller, H., Frege, C., Gonzalez-Carracedo, L., Gordon, H., Granzin, M., Hakala, J., Hofbauer, V., Hoyle, C. R., Kim, C., Kong, W., Lamkaddam, H., Lee, C. P., Lehtipalo, K., Leiminger, M., Mai, H., Manninen, H. E., Marie, G., Marten, R., Mentler, B., Molteni, U., Nichman, L., Nie, W., Ojdanic, A., Onnela, A., Partoll, E., Petäjä, T., Pfeifer, J., Philippov, M., Quéléver, L. L. J., Ranjithkumar, A., Rissanen, M. P., Schallhart, S., Schobesberger, S., Schuchmann, S., Shen, J., Sipilä, M., Steiner, G., Stozhkov, Y., Tauber, C., Tham, Y. J., Tomé, A. R., Vazquez-Pufleau, M., Vogel, A. L., Wagner, R., Wang, M., Wang, D. S., Wang, Y., Weber, S. K., Wu, Y., Xiao, M., Yan, C., Ye, P., Ye, Q., Zauner-Wieczorek, M., Zhou, X., Baltensperger, U., Dommen, J., Flagan, R. C., Hansel, A., Kulmala, M., Volkamer, R., Winkler, P. M., Worsnop, D. R., Donahue, N. M., Kirkby, J., and Curtius, J.: Molecular understanding of newparticle formation from a-pinene between -50 and +25 °C, Atmos. Chem. Phys., 20, 9183-9207, https://doi.org/10.5194/acp-20-9183-2020, 2020.
- Smith, J. N., Barsanti, K. C., Friedli, H. R., Ehn, M., Kulmala, M., Collins, D. R., Scheckman, J. H., Williams, B. J., and McMurry, P. H.: Observations of aminium salts in atmospheric nanoparticles and possible climatic implications, Proc. Natl. Acad. Sci. U. S. A., 107, 6634–6639, https://doi.org/10.1073/pnas.0912127107, 2010.
- Stolzenburg, D., Fischer, L., Vogel, A. L., Heinritzi, M., Schervish,
 M., Simon, M., Wagner, A. C., Dada, L., Ahonen, L. R., Amorim,
 A., Baccarini, A., Bauer, P. S., Baumgartner, B., Bergen, A.,
 Bianchi, F., Breitenlechner, M., Brilke, S., Mazon, S. B., Chen,

- D., Dias, A., Draper, D. C., Duplissy, J., El Haddad, I., Finkenzeller, H., Frege, C., Fuchs, C., Garmash, O., Gordon, H., He, X., Helm, J., Hofbauer, V., Hoyle, C. R., Kim, C., Kirkby, J., Kontkanen, J., Kürten, A., Lampilahti, J., Lawler, M., Lehtipalo, K., Leiminger, M., Mai, H., Mathot, S., Mentler, B., Molteni, U., Nie, W., Nieminen, T., Nowak, J. B., Ojdanic, A., Onnela, A., Passananti, M., Petäjä, T., Quéléver, L. L. J., Rissanen, M. P., Sarnela, N., Schallhart, S., Tauber, C., Tomé, A., Wagner, R., Wang, M., Weitz, L., Wimmer, D., Xiao, M., Yan, C., Ye, P., Zha, Q., Baltensperger, U., Curtius, J., Dommen, J., Flagan, R. C., Kulmala, M., Smith, J. N., Worsnop, D. R., Hansel, A., Donahue, N. M., and Winkler, P. M.: Rapid growth of organic aerosol nanoparticles over a wide tropospheric temperature range, Proc. Natl. Acad. Sci. U. S. A., 115, 9122–9127, https://doi.org/10.1073/pnas.1807604115, 2018.
- Tröstl, J., Chuang, W. K., Gordon, H., Heinritzi, M., Yan, C., Molteni, U., Ahlm, L., Frege, C., Bianchi, F., Wagner, R., Simon, M., Lehtipalo, K., Williamson, C., Craven, J. S., Duplissy, J., Adamov, A., Almeida, J., Bernhammer, A.-K., Breitenlechner, M., Brilke, S., Dias, A., Ehrhart, S., Flagan, R. C., Franchin, A., Fuchs, C., Guida, R., Gysel, M., Hansel, A., Hoyle, C. R., Jokinen, T., Junninen, H., Kangasluoma, J., Keskinen, H., Kim, J., Krapf, M., Kürten, A., Laaksonen, A., Lawler, M., Leiminger, M., Mathot, S., Möhler, O., Nieminen, T., Onnela, A., Petäjä, T., Piel, F. M., Miettinen, P., Rissanen, M. P., Rondo, L., Sarnela, N., Schobesberger, S., Sengupta, K., Sipilä, M., Smith, J. N., Steiner, G., Tomé, A., Virtanen, A., Wagner, A. C., Weingartner, E., Wimmer, D., Winkler, P. M., Ye, P., Carslaw, K. S., Curtius, J., Dommen, J., Kirkby, J., Kulmala, M., Riipinen, I., Worsnop, D. R., Donahue, N. M., and Baltensperger, U.: The role of low-volatility organic compounds in initial particle growth in the atmosphere, Nature, 533, 527-531, https://doi.org/10.1038/nature18271, 2016.
- Victor, J. N., Buchunde, P., Sebastian, M., Kanawade, V. P., Siingh, D., Mukherjee, S., Potdar, S. S., Dharmaraj, T., and Pandithurai, G.: Characteristics of new particle formation events in a mountain semi-rural location in India, Atmos. Environ., 324, 120414, https://doi.org/10.1016/j.atmosenv.2024.120414, 2024.
- Wang, Y., Yang, G., Lu, Y., Liu, Y., Chen, J., and Wang, L.: Detection of gaseous dimethylamine using vocus proton-transfer-reaction time-of-flight mass spectrometry, Atmos. Environ., 243, 117875, https://doi.org/10.1016/j.atmosenv.2020.117875, 2020.
- Xiao, M., Hoyle, C. R., Dada, L., Stolzenburg, D., Kürten, A., Wang, M., Lamkaddam, H., Garmash, O., Mentler, B., Molteni, U., Baccarini, A., Simon, M., He, X.-C., Lehtipalo, K., Ahonen, L. R., Baalbaki, R., Bauer, P. S., Beck, L., Bell, D., Bianchi, F., Brilke, S., Chen, D., Chiu, R., Dias, A., Duplissy, J., Finkenzeller, H., Gordon, H., Hofbauer, V., Kim, C., Koenig, T. K., Lampilahti, J., Lee, C. P., Li, Z., Mai, H., Makhmutov, V., Manninen, H. E., Marten, R., Mathot, S., Mauldin, R. L., Nie, W., Onnela, A., Partoll, E., Petäjä, T., Pfeifer, J., Pospisilova, V., Quéléver, L. L. J., Rissanen, M., Schobesberger, S., Schuchmann, S., Stozhkov, Y., Tauber, C., Tham, Y. J., Tomé, A., Vazquez-Pufleau, M., Wagner, A. C., Wagner, R., Wang, Y., Weitz, L., Wimmer, D., Wu, Y., Yan, C., Ye, P., Ye, Q., Zha, Q., Zhou, X., Amorim, A., Carslaw, K., Curtius, J., Hansel, A., Volkamer, R., Winkler, P. M., Flagan, R. C., Kulmala, M., Worsnop, D. R., Kirkby, J., Donahue, N. M., Baltensperger, U., El Haddad, I., and Dommen, J.: The driving factors of new parti-

- cle formation and growth in the polluted boundary layer, Atmos. Chem. Phys., 21, 14275–14291, https://doi.org/10.5194/acp-21-14275-2021, 2021.
- Xiao, S., Wang, M. Y., Yao, L., Kulmala, M., Zhou, B., Yang, X., Chen, J. M., Wang, D. F., Fu, Q. Y., Worsnop, D. R., and Wang, L.: Strong atmospheric new particle formation in winter in urban Shanghai, China, Atmos. Chem. Phys., 15, 1769–1781, https://doi.org/10.5194/acp-15-1769-2015, 2015.
- Yan, C., Yin, R., Lu, Y., Dada, L., Yang, D., Fu, Y., Kontkanen, J., Deng, C., Garmash, O., Ruan, J., Baalbaki, R., Schervish, M., Cai, R., Bloss, M., Chan, T., Chen, T., Chen, Q., Chen, X., Chen, Y., Chu, B., Dällenbach, K., Foreback, B., He, X., Heikkinen, L., Jokinen, T., Junninen, H., Kangasluoma, J., Kokkonen, T., Kurppa, M., Lehtipalo, K., Li, H., Li, H., Li, X., Liu, Y., Ma, Q., Paasonen, P., Rantala, P., Pileci, R. E., Rusanen, A., Sarnela, N., Simonen, P., Wang, S., Wang, W., Wang, Y., Xue, M., Yang, G., Yao, L., Zhou, Y., Kujansuu, J., Petäjä, T., Nie, W., Ma, Y., Ge, M., He, H., Donahue, N. M., Worsnop, D. R., Kerminen, V.-M., Wang, L., Liu, Y., Zheng, J., Kulmala, M., Jiang, J., and Bianchi, F.: The synergistic role of sulfuric acid, bases, and oxidized organics governing new-particle formation in Beijing, Geophys. Res. Lett., 48, e2020GL091944, https://doi.org/10.1029/2020GL091944, 2021.
- Yao, L., Wang, M.-Y., Wang, X.-K., Liu, Y.-J., Chen, H.-F., Zheng, J., Nie, W., Ding, A.-J., Geng, F.-H., Wang, D.-F., Chen, J.-M., Worsnop, D. R., and Wang, L.: Detection of atmospheric gaseous amines and amides by a high-resolution timeof-flight chemical ionization mass spectrometer with protonated ethanol reagent ions, Atmos. Chem. Phys., 16, 14527–14543, https://doi.org/10.5194/acp-16-14527-2016, 2016.
- Yao, L., Garmash, O., Bianchi, F., Zheng, J., Yan, C., Kontkanen, J., Junninen, H., Mazon, S. B., Ehn, M., Paasonen, P., Sipila, M., Wang, M., Wang, X., Xiao, S., Chen, H., Lu, Y., Zhang, B., Wang, D., Fu, Q., Geng, F., Li, L., Wang, H., Qiao, L., Yang, X., Chen, J., Kerminen, V.-M., Petäjä, T., Worsnop, D. R., Kulmala, M., and Wang, L.: Atmospheric new particle formation from sulfuric acid and amines in a Chinese megacity, Science, 361, 278–281, https://doi.org/10.1126/science.aao4839, 2018.

- Yin, R., Yan, C., Cai, R., Li, X., Shen, J., Lu, Y., Schobesberger, S., Fu, Y., Deng, C., Wang, L., Liu, Y., Zheng, J., Xie, H., Bianchi, F., Worsnop, D. R., Kulmala, M., and Jiang, J.: Acid-base clusters during atmospheric new particle formation in urban Beijing, Environ. Sci. Technol., 55, 10994–11005, https://doi.org/10.1021/acs.est.1c02701, 2021.
- Yu, H., Zhou, L., Dai, L., Shen, W., Dai, W., Zheng, J., Ma, Y., and Chen, M.: Nucleation and growth of sub-3 nm particles in the polluted urban atmosphere of a megacity in China, Atmos. Chem. Phys., 16, 2641–2657, https://doi.org/10.5194/acp-16-2641-2016, 2016.
- Zhao, B., Donahue, N. M., Zhang, K., Mao, L., Shrivastava, M., Ma, P.-L., Shen, J., Wang, S., Sun, J., Gordon, H., Tang, S., Fast, J., Wang, M., Gao, Y., Yan, C., Singh, B., Li, Z., Huang, L., Lou, S., Lin, G., Wang, H., Jiang, J., Ding, A., Nie, W., Qi, X., Chi, X., and Wang, L.: Global variability in atmospheric new particle formation mechanisms, Nature, 631, 98–105, https://doi.org/10.1038/s41586-024-07547-1, 2024.
- Zhou, Y., Hakala, S., Yan, C., Gao, Y., Yao, X., Chu, B., Chan, T., Kangasluoma, J., Gani, S., Kontkanen, J., Paasonen, P., Liu, Y., Petäjä, T., Kulmala, M., and Dada, L.: Measurement report: New particle formation characteristics at an urban and a mountain station in northern China, Atmos. Chem. Phys., 21, 17885–17906, https://doi.org/10.5194/acp-21-17885-2021, 2021.